High-frequency microrheology of wormlike micelles

M. Buchanan,[1,2] M. Atakhorrami,[1] J. F. Palierne,[3] F. C. MacKintosh,[1] and C. F. Schmidt[1]

[1]*Department of Physics and Astronomy, Vrije Universiteit Amsterdam, The Netherlands*
[2]*Physics of Geological Processes, Department of Physics, University of Oslo, Norway*
[3]*Laboratoire de Physique, Ecole Normale Suprieure de Lyon, France*

We have measured the frequency-dependent shear modulus of entangled solutions of wormlike micelles by high-frequency microrheology and have compared the results with those from macrorheology experiments done on the same samples. Using optical microrheology based on laser interferometry we have measured loss and storage moduli over six decades in frequency up to about 100 kHz. We present data over a decade in concentration in the entangled regime and find good agreement between micro- and macrorheology, thus validating recently developed microrheology techniques. By collapsing data for different concentrations, we furthermore determine both the concentration scaling of the plateau modulus and a power-law exponent of the complex shear modulus at high frequencies.

I. INTRODUCTION

Microrheology is a powerful new technique for studying the viscoelastic properties of complex fluids and soft materials with high bandwidth and spatial resolution [1–8]. To determine the viscoelastic behavior of a particular system using this technique one must employ a number of assumptions and subtle physical approximations in evaluating the data. Until now a rigorous comparison between established conventional rheology and microrheology on a stable, well-known system has been lacking. Here we set out to provide such a comparison using entangled solutions of wormlike micelles.

Microrheology techniques are based on tracking the motions of micron-sized probe particles embedded in the system to be studied. Variations of the technique include active and passive methods, as well as single- and multiple-particle methods [8]. In the passive methods, such as the one applied here, the fluctuation-dissipation theorem of linear response theory [9] is used to extract viscoelastic parameters [5,6,8,10] of the material from the thermal equilibrium fluctuations of the embedded particles. In contrast to typical macroscopic mechanical rheology, no strain is applied to the material during the measurement, and linear response parameters can be measured directly without extrapolation. This is particularly useful in soft materials and complex fluids where even a small imposed strain can cause reorganization of structure within the material and thus change its viscoelastic properties (e.g., strain hardening or shear thinning). Furthermore, when using micron-sized probes, probe and solvent inertial effects are largely negligible up to frequencies of 100 kHz. Microrheology thus achieves a bandwidth far beyond that of conventional macroscopic rheometers, with the exception of specialized designs, such as ones using resonant probes [11,12] or the instrument we use here for comparison, which is based on piezoelectric actuators and reaches 10 kHz [13].

In contrast to common instruments such as plate-and-cone rheometers, there is no constant-volume constraint on the medium around the probe in microrheology. Therefore the probe motions can couple to pure shear modes as well as to compressional modes. This opens a new window to study the latter in complex fluids, but it also complicates the comparison with macrorheology, especially at low frequencies. If the material studied is a polymer solution, the viscoelastic response measured by microrheology will asymptotically approach pure shear response due to the viscous coupling of polymer to solvent at higher frequencies [6,14–16].

The thermal motion of a single particle reflects the viscoelastic properties of its environment on roughly the scale of the probe particle radius since this is the length scale on which the strain-field around the particle decays [6,17]. This sets the spatial resolution of the method and therefore results in micrometer resolution for micrometer particles. Ideally one wants to measure material properties that are not perturbed by the presence of the probe particle itself. From the preceding argument it is evident that this will not be the case if the particle perturbs the medium on a length scale comparable to its radius. The probe can influence the material near its surface in several ways, e.g., by physical *entropic* depletion or by chemical or electrostatic interaction with the material. How deep into the material such a perturbation propagates depends on the characteristic length scales of the material in relation to the probe size. If the probe particle is smaller than material scales (such as polymer persistence length, contour length, Debye length, etc.), perturbations will decay over a distance of order the probe size and true bulk properties are not measured. If all material scales are smaller than the particle, surface effects should be negligible. Biopolymer solutions and gels made of, for example, filamentous actin [6,7], DNA [18], or polysaccharides [7] typically have intrinsic length scales as large as a micrometer. In this case it may be insufficient to analyze the fluctuations of an isolated probe particle. A way to avoid probe effects and determine the bulk viscoelastic behavior in these cases is to measure the correlated fluctuations of pairs of particles separated by more than the relevant material length scales (two-particle microrheology) [7,19]. In this study we have selected a system with small characteristic length scales, so

that single-particle microrheology should not be influenced by local surface effects.

The polymer system studied here was an entangled solution of wormlike micelles. Wormlike micelles are cylindrical assemblies of amphiphilic molecules that form spontaneously in aqueous solutions at particular concentrations and temperature conditions. Their properties have been well studied, both experimentally and theoretically [20–22]. We have used cetylpyridinium chloride (CPyCl) as the surfactant and sodium salicylate (NaSal) as a strongly binding counterion. The wormlike micelles formed in this system have a diameter of 2 to 3 nm, contour lengths of 100 nm–1 μm, and a persistence length of order 10 nm [20]. At the concentrations we used (1–8 wt %), the mesh size varies from about 30 to 10 nm [22].

Despite their rather exotic structure and dynamics, wormlike micelles exhibit well-defined rheological properties, similar to those of covalently linked linear polymers. When entangled wormlike micelles are sheared, relaxation of stress occurs via reptation and scission [23]. Both processes, occurring simultaneously, lead to a single dominating relaxation time being observed. Systems with one relaxation time are known as Maxwell fluids and have been studied extensively [22,24]. In general, studies performed on wormlike micelles have focused on low-frequency properties where the simple mechanical analog, the Maxwell model, consisting of a dashpot and a spring in series, can be used to model the viscoelastic response. Higher frequency rheology has been performed on micelle systems confirming the Maxwell regime at somewhat elevated frequencies [25,26].

We have chosen wormlike micelle solutions as a model system to quantitatively test the underlying principles of microrheology and to provide a benchmark performance test. Specifically, we have performed detailed comparisons between single particle microrheology and a macroscopic technique using a piezorheometer [13] over a frequency range from 0.1 Hz to about 10 kHz. We have performed experiments with both techniques for micelle solutions covering a range of shear moduli ranging from 1 to 200 Pa at low frequency. Our results demonstrate excellent agreement between the two techniques and make a strong case for the validity of single-particle microrheology for soft materials with intrinsic length scales below the probe size. At high frequencies the (single relaxation time) Maxwell model does not apply anymore and internal micelle dynamics become important, presenting a continuous spectrum of relaxation times. We introduce simple scaling arguments to interpret the high-frequency dynamic properties of micelle solutions in a regime where collective network dynamics cross over to single filament dynamics.

This paper is organized as follows. In Sec. II, we present the theoretical background and cover some fundamental aspects of microrheology and data evaluation. In Sec. III we outline the experimental procedure, sample preparation, and how data are collected and analyzed. In Sec. IV we present our results, comparing microrheology and macrorheology and investigating the scaling behavior of the shear moduli at high and low frequencies. In Sec. V we discuss the results.

II. THEORETICAL BACKGROUND

In optical microrheology, the complex viscoelastic modulus, $G = G' + iG''$ can be obtained from direct measurement of the displacement fluctuations of micrometer size dielectric particles [2,5,6]. By relying on fundamental principles such as the fluctuation-dissipation theorem [9,27], one can in many cases obtain the frequency-dependent shear modulus G of materials in this way.

In a general viscoelastic material, the position x of an embedded particle is related, within the linear regime, to the applied force f by a response function α via $x_\omega = \alpha(\omega)f_\omega$. Here, the various quantities represent complex Fourier transforms, and thus depend on frequency ω. In particular, the response function itself is complex, exhibiting both storage (elasticlike) and loss (dissipative or viscouslike) character for viscoelastic materials.

In the absence of any externally applied forces, random thermal or Brownian forces will give rise to fluctuations of the particle position. These fluctuations are fundamentally related to the temperature of the system and the response function or compliance α via the fluctuation-dissipation theorem [9,27]. One common expression of the (classical) fluctuation-dissipation theorem relates the power-spectral-density (PSD) $\langle |x_\omega|^2 \rangle$ of particle fluctuations to the imaginary part of the response function $\alpha'' = \text{Im}(\alpha)$:

$$\langle |x_\omega|^2 \rangle = \frac{2kT}{\omega} \alpha''(\omega). \tag{1}$$

In our experiments, we measure the power spectral density (PSD) of the displacement fluctuations, which is then directly used to determine the imaginary response function, as shown above. In addition to the fluctuation-dissipation theorem, linear response theory also shows that the real and imaginary parts of the response function α can be obtained from each other. Specifically, provided that the PSD, and thus $\alpha''(\omega)$, can be determined over a wide frequency range, it is possible to determine the real part $\alpha'(\omega)$ using a Kramer-Kronig relation

$$\alpha'(\omega) = \frac{2}{\pi} \int_0^\infty \frac{\xi \alpha''(\xi)}{\omega^2 + \xi^2} d\xi. \tag{2}$$

We use numerical integration to obtain the real part of the compliance, and thus the full, complex α. In an incompressible, linear viscoelastic medium, the geometry-dependent compliance is related to the complex shear modulus $G(\omega) = G' + iG''$ of the embedding medium via [5,6]

$$G(\omega) = \frac{1}{6\pi R \alpha(\omega)}. \tag{3}$$

In principle, the integral in the Kramers-Kronig relation above must be performed out to infinite frequency. In practice, however, one has only a finite data set for the PSD, and thus $\alpha''(\omega)$. Due to the finite range of the KK integral $\alpha'(\omega)$ will be slightly underestimated. By evaluating the integral above assuming $\alpha''(\omega)$ continues to infinity with a slope of −1 (i.e., as for a simple viscous liquid), we can obtain an analytic correction. Although not necessarily physically cor-

rect, it allows us to estimate how much of an effect the finite data set has. Specifically, we assume that $\alpha''(\omega)$ continues from the Nyquist frequency ω_N with a slope of -1. Thus $\alpha''(\omega) = \alpha''_N \omega_N / \omega$ where the numerator is determined from the data. By integrating this part from ω_N to infinity one obtains a frequency-dependent correction of $\alpha'(\omega)$.

$$\alpha'_c(\omega) = -\frac{\alpha''_N \omega_N}{\omega} \ln \left| \frac{\omega_N - \omega}{\omega_N + \omega} \right|. \qquad (4)$$

This correction may lead to an underestimate of both $G'(\omega)$ and $G''(\omega)$ for the higher concentration data where the correction is large (see Fig. 4). If high accuracy is desired in this range, data should be taken at high sampling rates at the cost of large memory usage.

In an incompressible medium, the response function is related to the (complex) shear modulus G by the generalized Stokes-Einstein relation in Eq. (3). Using this we can extract the storage and loss moduli $G'(\omega)$ and $G''(\omega)$ from the response functions $\alpha'(\omega)$ and $\alpha''(\omega)$, via

$$G'(\omega) = \frac{1}{6\pi R} \left(\frac{\alpha'(\omega)}{\alpha'(\omega)^2 + \alpha''(\omega)^2} \right) \qquad (5)$$

and

$$G''(\omega) = \frac{1}{6\pi R} \left(\frac{-\alpha''(\omega)}{\alpha'(\omega)^2 + \alpha''(\omega)^2} \right). \qquad (6)$$

III. EXPERIMENTAL METHODS

A. Materials

Wormlike micelles were prepared from the surfactant cetylpyridinium chloride (CPyCl) dissolved in brine (0.5 M NaCl) with strongly binding counterions, sodium salicylate (NaSal). Chemicals were obtained from Sigma Chemical Co. (Sigma-Aldrich Chemie B.V. Zwijndrecht, The Netherlands). In this study all samples have a molar ratio Sal/CPy=0.5. A tiny quantity, below 10^{-3} vol %, of silica particles with a diameter of 0.98 μm (Bangs Laboratories, Fishers, IN) was added to each sample before measurement. The micellar solutions were stored at (controlled) ambient temperature (between 21.5 and 22.0 °C) which was above the Krafft point of this system.

B. Macrorheology

A custom-built piezorheometer [13] was used to measure the viscous and elastic shear moduli of wormlike micelle samples prepared in parallel with the ones used for microrheology. Details of this technique can be found in the literature [28]. Briefly, samples are contained between two glass plates mounted horizontally between two piezoelectric ceramics. One of the plates is sinusoidally oscillated with a vertical amplitude of about 1 nm. This movement squeezes the sample and causes mainly shear strain with some extensional flow in the very center of the sample. The vertical stress transmitted to the second plate is measured by the other piezoelectric element. The imposed strain is extremely small

so that the sample structure is not altered by the flow. This instrument allowed us to measure the storage (G') and loss (G'') shear modulus for frequencies ranging from 0.1 Hz to 10 kHz. The temperatures at which we measured were 21.8 °C for c_p=1 and 2%, 22.4 °C for c_p=4%, 22.6 °C for c_p=5 and 8%, and 22.0 °C for c_p=6%. The setup was hermetically sealed to avoid evaporation.

C. Microrheology

All microrheology experiments were performed on a custom-built optical microscope equipped with differential interference contrast optics and with optical traps essentially as described earlier [6,29]. Briefly, an infrared laser (λ =1064 nm, NdVO$_4$, COMPASS, Coherent, Santa Clara, CA) was coupled into the sample via the microscope objective lens (Zeiss, Neofluar, 100×, NA=1.3) with immersion oil (n_{oil}=1.5, Cargille LTD, Cedar Grove, NJ) and used to trap particles. A quadrant photodiode (YAG444-4A, Perkin Elmer, Vaudreuil, Canada) was used to measure the lateral (x and y) displacements of the trapped particle relative to the laser focus by back-focal-plane interferometry [30]. In this detection scheme the back-focal plane of the condenser (Zeiss, NA=1.4, oil) collecting the laser light after the interaction with the probe particle is imaged onto the quadrant photodiode. The diode current signals are amplified by a low-noise analog differential amplifier (custom built), then digitized with a 200 kHz analog-to-digital board (AD16 board on a /ChicoPlus PC-card, Innovative Integration, Simi Valley, CA) and processed and stored on hard disk using Labview (National Instruments, Austin, TX). Time-series data were stored and later (off-line) calibrated to displacement in nm as described below, using independently measured calibration factors from particles trapped in water samples. We can track particle motions with a bandwidth of about 100 kHz in our setup [31].

The laboratory temperature was stabilized to between 21.5 and 22.0 °C. Micelle samples were doped with silica particles as described above and then introduced into a sample chamber. Sample chambers were assembled of a microscope slide and a coverslip separated by spacers of double-stick tape and sealed with grease (Apiezon L, M&I Materials Ltd, Manchester, U.K.). The inner height of the sample chambers was about 70 μm. Probe particles were trapped and were moved to about 20 μm above the glass surface. In order to ensure that the samples were completely relaxed and isotropic after the filling procedure and the probe positioning, x (aligned with the long axis of the chamber) and y fluctuations were measured, and averaged power spectral densities (PSD) of 60 s segments of data were obtained. The instrument was aligned before each set of experiments and, among other criteria, it was tested that x and y PSDs of beads trapped in pure solvent were overlapping. Immediately after manipulating the wormlike micelles samples, x and y PSDs were not overlapping, with the x spectra (in the flow direction) typically showing a higher rms amplitude of motion than the y spectra, due to shear-induced structural changes in the solutions. After typically about 15 min, PSDs overlapped and we used this as a criterion that the samples had come to equilibrium.
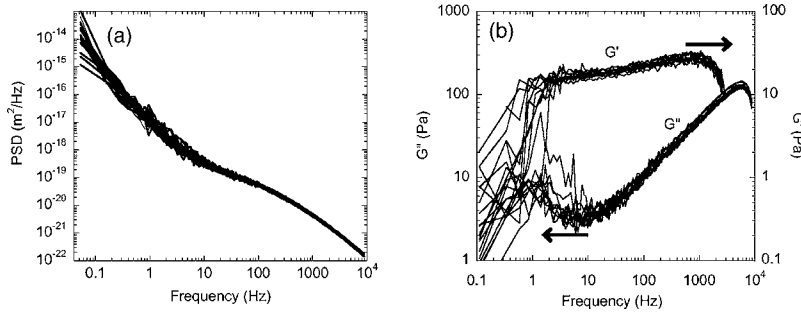
FIG. 1. Power spectral densities (PSD) of thermal bead motion in a wormlike micelle solution (a), and storage (G') and loss (G'') modulus of the solution derived from the PSDs (b). The scatter in amplitude and shape of the curves illustrates reproducibility for 16 different runs using three different beads ($d=0.98$ μm) in the same sample ($c_p=4\%$). The vertical axes for G' and G'' in (b) are shifted apart for visibility.

For each sample, once they had fully relaxed, we obtained between 8 and 16 data sets. Each data file was about 5 MB. In most samples eight data sets were sufficient, however, in the high concentration samples up to 16 runs were required to obtain better averaging and to reduce noise in the data. For each sample we measured at two different sample frequencies. Careful attention was paid to checking for anisotropic behavior (difference in x and y PSDs) that occasionally occurred due to the movement of small air bubbles or a leak in the chamber. Data sets that showed anisotropic behavior were eliminated. Figure 1 shows a typical set of data to illustrate reproducibility from run to run with different beads. PSDs were then averaged for all beads in the sample and for x and y directions, before shear elastic parameters were calculated.

Data were taken at two sample rates in order to cover maximum bandwidth. To capture the low-frequency end of the spectrum, we sampled at 20 kHz and recorded for 60 s (0.1 to 10 kHz bandwidth). In order to minimize the elastic contribution from the trap we used a low laser power of $\sim$3 mW which gave a trap stiffness of 1.6 pN/nm (measured in buffer), resulting in an apparent added constant of G' $\sim$0.1 Pa in the final result for the shear moduli. The trap effect was corrected for by subtracting this constant [32]. At the high sampling rate of 195 kHz a higher power of $\sim$30 mW was required to avoid shot noise, which resulted in a correction of $G' \sim 1$ Pa. Shot noise is visible as a *turning-up* of the PSD at high frequencies. At both high and low laser powers heating of the sample due to the laser was estimated to be less than 1 °C and therefore considered negligible [33]. Time series data were further processed off-line on a PC, using LabView software to obtain the real and imaginary part of the complex shear modulus of the wormlike micelle solutions according to Eqs. (5) and (6). Final results were smoothed by logarithmic binning with a factor of 1.05 relating the widths of successive bins. Data were thus averaged into N bins where N is determined by the algorithm $N=\log_{1.05}(n/100)$ where n is the total number of data points before binning.

Calibration factors to convert stored voltage time-series data to actual displacement time series were determined from measurements of the PSDs of the same beads as used in the wormlike micelle experiments in water. PSDs of beads trapped in a purely viscous fluid have a Lorentzian shape and from the amplitude of the Lorentzian at high frequencies, calibration factors can be determined if bead size, solvent viscosity, and temperature are used as (given) parameters [34]. Silica beads in water were trapped 20 μm from the

glass surface at both the low and high laser power used in the micelle experiments, and their displacement fluctuations were measured at sampling rates of 20 and 195 kHz, respectively. Typically the x- and y-position components of three or more particles were measured and an average PSD was obtained [34]. The variance on these runs is approximately 5% which is likely mainly due to bead polydispersity (compare with Fig. 1).

IV. RESULTS

Microrheology experiments on flexible wormlike micelles were performed in the semidilute regime ($c > c^*$ $\sim$ 0.3 wt %) where the micelles are entangled. The entanglement length has been reported to vary between 30 and 10 nm for $c_p=1-8$ wt %, respectively [22].

A. Comparing microrheology and macrorheology

Figure 2 shows the PSDs for water and wormlike micelle solutions at $c_p=1$, 2, 4, 5, 6, and 8 wt %. Following the procedure outlined above real and imaginary parts of the complex compliance were determined by use of a Kramers-Kronig integral [9]. Frequency-dependent viscoelastic moduli were then calculated from the compliance and corrected for the trapping effect as described. Figure 3 shows the effect of correcting the compliance for the finite high-
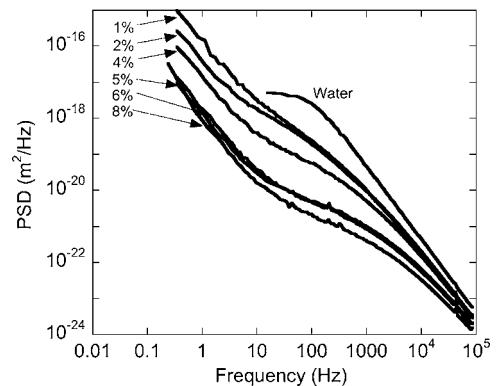
FIG. 2. Power spectral densities of displacement fluctuations for 0.98 μm diameter beads in water and in wormlike micelle solutions of concentrations, $c_p=2$, 4, 6, and 8 wt %. PSDs are each an average of eight spectra recorded from three different beads in the respective sample, smoothed by logarithmic binning. Data were taken for each concentration at 20 and 195 kHz sampling rates and were merged for each concentration.
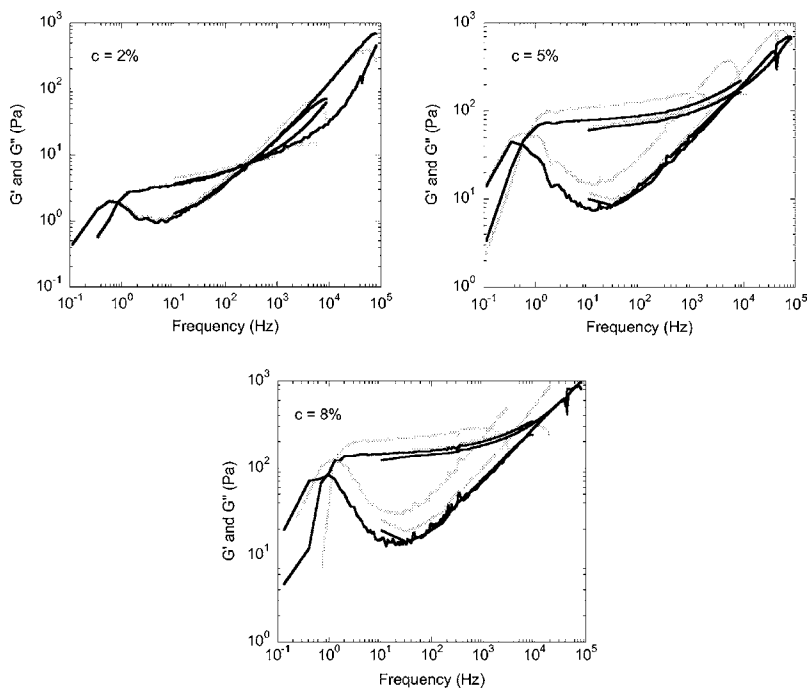
FIG. 3. Comparison of complex shear moduli of wormlike micelle solutions of concentrations $c_p=2$, 5, and 8 wt %, uncorrected (gray lines) and corrected (black lines) for the finite high-frequency cutoff of the Kramers-Kronig integral. Moduli were measured by microrheology with probe particles of 0.98 μm diameter at 20 and 195 kHz sampling rates. The correction effect is more pronounced for low sampling rates and high concentrations. Data curves are averages of eight spectra recorded from three different beads in each case, smoothed by logarithmic binning.

frequency cutoff of the Kramers-Kronig integral on the final results for the shear elastic moduli, G' and G'', as described above. Gray lines are uncorrected and black lines are corrected storage and loss moduli for concentrations $c_p=2$, 5, and 8 wt %. At high concentrations and low sampling rates the correction is significant, while at high sampling rates it is minor. In the following, only corrected curves are presented.

Shear moduli obtained from the fluctuation analysis of 0.98 μm diameter beads, averaged over about three beads in each case, and macrorheology data obtained with the piezorheometer are presented in Fig. 4 for micelle concentrations $c_p=1$, 2, 4, 5, 6, and 8 wt %. Each panel shows a comparison between shear elastic moduli, derived from macrorheology (symbols) and microrheology (lines) for
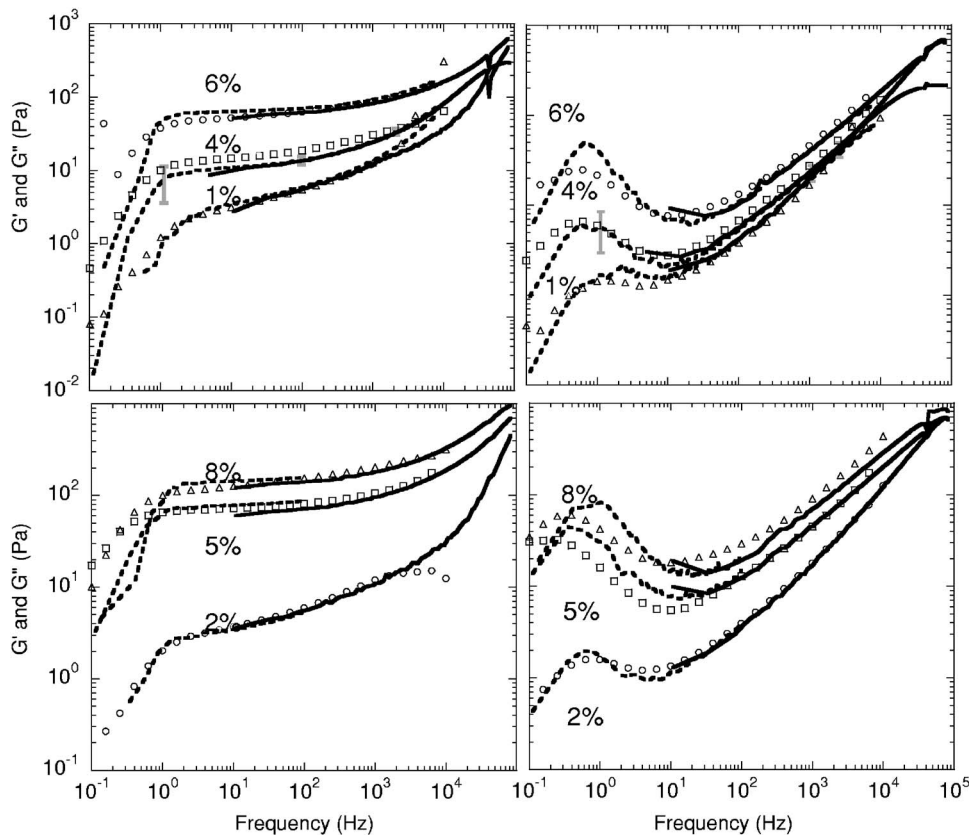
FIG. 4. Complex shear moduli (G' on the left, G'' on the right) for wormlike micelle solutions of concentrations $c_p=1$, 2, 4, 5, 6, and 8 wt % as labeled in the plots. Lines are microrheology results with probe particles of 0.98 μm diameter (solid line 195 kHz sampling rate, dashed line 20 kHz sampling rate). Data were averaged from eight recorded spectra from three different beads, smoothed by logarithmic binning. Symbols are macrorheology results obtained with the piezorheometer.
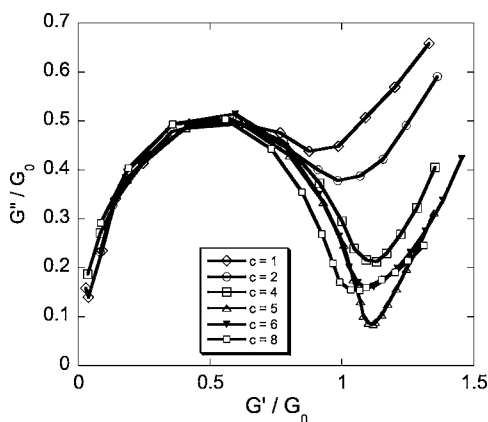
FIG. 5. Cole-Cole plot of normalized viscous modulus against normalized elastic modulus for wormlike micelle solutions of concentrations $c_p=1$, 2, 4, 5, 6, and 8 wt %, measured with the piezorheometer on macroscopic samples. Data curves follow Maxwell behavior at low frequencies.

three concentrations. Storage moduli, G', are plotted on the left, and loss moduli, G'', on the right. Microrheology data were taken at two different sampling rates: 195 kHz (solid lines) and 20 kHz (dashed line).

Over a large range of concentrations excellent agreement between microrheology and macrorheology is observed. For the microrheology data the low frequency data are taken at a lower sampling frequency and lower power allowing us access to the lower frequency range. Due to the extended time required for these runs and the increase in noise in the data it is important to verify an overlap of data with the high sampling rate data. In our data excellent agreement over a decade in the midrange frequency region between high and low sampling rate runs is observed.

B. Scaling behavior and high-frequency viscoelasticity

Maxwell behavior in the low-frequency regime for viscoelastic fluids is usually demonstrated in a Cole-Cole plot of normalized loss modulus plotted against normalized storage modulus (Fig. 5). With a single relaxation time t^*, the moduli become: $G(\omega)=i\omega\nu_0/(1+i\omega t^*)$ where the zero time shear modulus is $G_\infty=\nu_0/t^*$, which will result in a half-circle with radius 0.5 in the Cole-Cole plot. Our data demonstrate this behavior (see Fig. 5) at the low-frequency end of the moduli. The relaxation times can be determined from the crossovers of G' and G'' in Fig. 6.

Deviations from the circle reflect additional internal dynamics of the micelles [35]. At the high-frequency end these will be dominated by the bending fluctuations of individual micelles which lead to a continuum of relaxation times, commonly resulting in a power-law form of the moduli [36,37].

The elastic plateau in $G'(\omega)$ reflects the collective dynamics of the entangled micelles and is maintained for frequencies above $1/t^*$ until the largest characteristic microscopic time scale of the system is reached, which is typically the relaxation time of a single mesh in a flexible polymer network. In simple physical terms, this crossover separates the plateau regime caused by collective network dynamics from
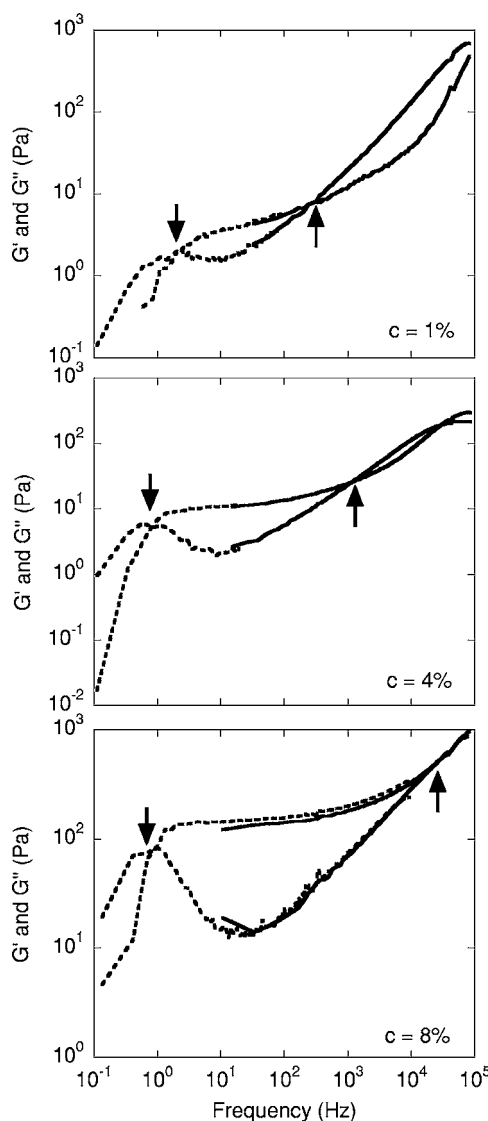
FIG. 6. Crossover frequencies: Storage and loss shear moduli were measured for wormlike micelle solutions of concentrations $c_p=1$, 4, and 8 wt % by microrheology with probe particles of 0.98 μm diameter (solid line 195 kHz sampling rate, dashed line 20 kHz sampling rate). Moduli are plotted (without shifting curves apart) to identify the crossover points of the two moduli. As concentration increases the high-frequency crossover moves to higher frequency indicated by upwards pointing arrows, while the low-frequency crossover moves to lower frequencies. Curves are at each concentration averages of eight spectra recorded from three different beads, smoothed by logarithmic binning. Frequencies for the high-frequency crossovers are 316, 1144, and 60 000 Hz.

the single-filament regime (e.g., Rouse behavior of flexible polymers) at higher frequencies [36]. The increase of the complex shear modulus at high frequencies can be understood as a progressive reduction of the compliance of individual filaments under periodic stress with increasing frequency. The compliance mainly arises from the relaxation of lateral undulation modes. Such modes typically exhibit a power-law dispersion, with relaxation time decreasing with wavelength, leading to power-law behavior of the shear modulus. In rheology, crossovers such as this one can be

extremely broad, covering many decades in frequency. It is evident from our data (Fig. 4) that, particularly for the more concentrated solutions, the high-frequency scaling regime is not reached within the bandwidth of our experiments.

The mesh size of the entangled solution decreases with increasing polymer concentration and the crossover frequency marking the end of the plateau is expected to rise accordingly. The plateau value of G' itself also increases with polymer concentration. Both effects can be seen in Fig. 6. In fact, these two effects are not independent, as is demonstrated empirically in Fig. 7. We can make these ideas more precise, and actually infer the characteristics of the high-frequency scaling regime from carefully analyzing the transition regime as follows. The approach is to collapse both the G' and G'' curves simultaneously by rescaling the frequency and moduli axes. This is similar to what was done in Ref. [38] for colloidal gels, but we must account for the single-filament bending dynamics of the micelles [39].

We consider a simple model describing both the plateau and the high-frequency regimes. The storage modulus is assumed to behave at low frequencies as

$$G'(\omega) \sim c_p{}^y, \qquad (7)$$

while both real and imaginary parts of the high-frequency modulus are assumed to increase with frequency ω according to

$$G'(\omega) \sim G''(\omega) \sim c_p \omega^z. \qquad (8)$$

In simple terms, we assume that the complex viscoelastic response of semidilute micelle solutions has two distinct contributions: (1) a frequency-independent component dominated by $G'(\omega)$ at low frequencies, and (2) a high-frequency component due to the relaxation of polymer between entanglements. The former represents the plateau, which is expected to depend on network architecture, e.g., the mesh size. It is expected to increase with concentration as a power-law with the exponent y that is left as a fit parameter. The latter, being a single-filament effect, is expected to depend linearly on concentration c_p.

For flexible polymers, the exponent z is expected to be in the range 0.5–0.7, depending on hydrodynamic interactions [36]. Following Ref. [38], we collapse the family of frequency-dependent shear moduli by introducing scaling factors $a(c)$ and $b(c)$ for each pair of G' and G'' curves at a given concentration, chosen for the best empirical collapse of the data. The G' and G'' graphs were scaled after water $G'' = \omega \eta_{\text{water}}$ was subtracted from the G''. The data collapse was done independently for both microrheology and macrorheology data [Figs. 7(a) and 7(b)].

Specifically, we chose the intermediate data set for 4% as a reference, and rescaled the modulus as bG and frequency as af for each of the other data sets for concentrations 1%, 2%, 5%, 6%, and 8% to match the 4% data. This method is sufficient since we are only interested in the scaling of the scaling factors. Assuming the model with exponents y and z expressed above, this means that $b \sim c_p^{-y}$ and that $a \sim c_p^{(1-y)/z}$, which means that $bc_p \sim a^z$. Thus by plotting $c_p b(c)$ versus $a(c)$, we expect a power-law relationship between the scaling
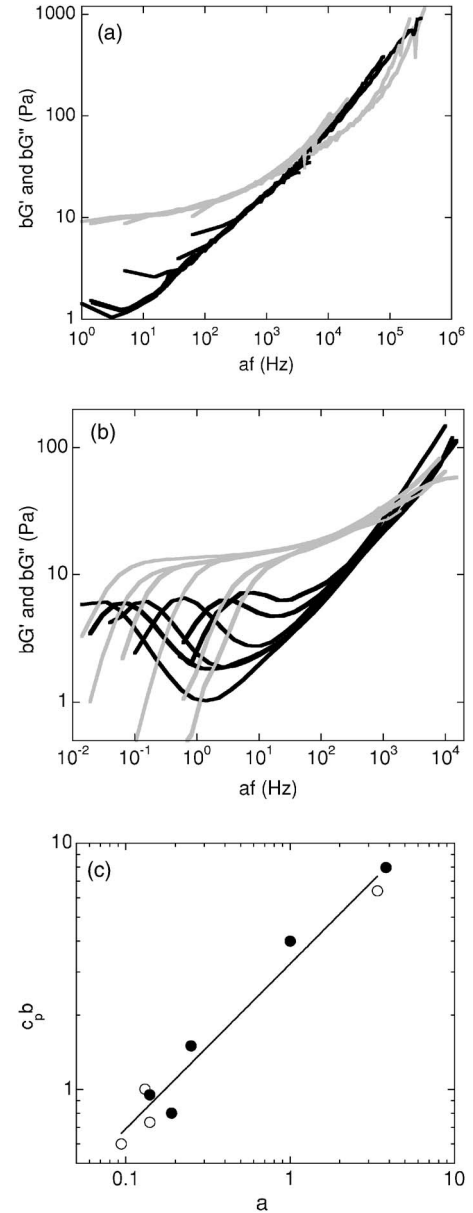
FIG. 7. Scaling analysis of storage and loss moduli: Scaling factors a and b were determined for every set of G' and G'' curves such that bG' and bG'' vs af collapse onto the respective 4% reference curves. (a) Moduli from microrheology with probe particles of 0.98 μm diameter for wormlike micelle solutions of concentrations c_p=1, 2, 4, 5, 6, and 8 wt %. (b) Macrorheology results (piezorheometer) for samples from the same stocks. (c) Plot of bc vs a to extract the high-frequency scaling exponent z of both moduli and the concentration scaling exponent of G' in the plateau regime. Filler data points are macrorheology and unfilled are microrheology.

factors, with the high-frequency scaling exponent z. The exponent z was found to be 0.67 from the combined plot of factors derived from macro- and microrheology [Fig. 7(c)]. The exponent y was calculated to be 1.89. At the low-frequency end the scaling is observed to break down as one approaches the Maxwell regime. This is expected because the terminal relaxation is not included in the model assumption of Eqs. (7) and (8).

V. DISCUSSION

For wormlike micelles the characteristic length scales of both individual micelles (diameter $\simeq 3$ nm, persistence length $\simeq 10$ nm) and of the polymer solution (mesh size $\simeq 30$ nm) are much smaller than the probe particle size. Furthermore, at the ionic strength of the brine we used, charge interactions are effectively screened with a Debye screening length of about 0.4 nm (0.5 M NaCl). Therefore single-particle microrheology should report correct bulk shear moduli. Consistent with this expectation, our experimental results (Figs. 3 and 4) show excellent agreement between single particle and mechanical rheology. This result verifies both the microrheology technique with the calibration and data evaluation procedures we used here as well as the assumptions involved. In particular, the assumption of strong coupling between polymer and solvent, limiting the dynamics to incompressible shear, appears to be justified down to the lowest frequencies we measured of 10^{-2} Hz. A deviation from strong coupling should have shown up as a growing decrease of the microrheology-moduli below the macrorheology values towards low frequencies. No such systematic difference was observed. On the other hand, a change of the Poisson ratio from 1/2 even all the way to 0 would only cause a slight decrease ($\sim 5\%$) of the shear modulus. Such an effect is difficult to resolve due to noise at low frequencies.

In some systems with relatively large internal characteristic length scales, the presence of the particle will locally affect the embedding medium so strongly that shear elastic moduli derived from single-particle microrheology will differ from average bulk values [26,40]. In particular, we have also performed similar experiments with the filamentous fd virus [41], and with the cytoskeletal protein actin [42], in the first case although the persistence length of fd is about 1 μm and comparable to bead sizes used, there was no measurable difference between one- and two-particle microrheology. In the second case (actin), there were strong probe particle effects at low and high frequencies [42]. In such cases, if spatial resolution and high bandwidth are desired, two-particle microrheology should be used. The price to pay is increased noise and that of a more complex experimental setup. Even in a system with small characteristic scales, slip boundary conditions have been suggested as a possible explanation for the discrepancies observed between one- and two-particle microrheology [40]. It is important that we have here found good agreement between single-particle microrheology and macrorheology in a simple system. This unambiguously proves the foundations of the technology and makes it now possible to quantitatively exploit the unique strengths of microrheology to study less simple systems. Apart from seeing effects created by the presence of the probe particle itself (which in themselves can be interesting), microrheology can be used, e.g., to map microscopic inhomogeneities, to study local nonaffine (bending) deformations of semiflexible or bundled polymers, or to measure low-frequency compressional elasticity of a polymer solution. In other words, what from one point of view might have been seen as a disadvantage of this technique, namely that results do not always agree with conventional rheology, is clearly emerging as an advantage providing more experimental access to phenomena that could not be studied with conventional rheology. One can, however, confidently exploit the capabilities of microrheology that go beyond those of conventional rheology only after it has been shown that agreement can be reached in simple systems, which we have done here.

The second result presented here is the high-frequency rheology data extending beyond the Maxwell regime. Earlier macrorheological work [24] had been technically limited to about 5 Hz. At high frequencies we expect an asymptotic crossover from elastic response determined by collective network dynamics to response dominated by short-range single-filament relaxation. The crossover frequency is expected to be concentration dependent, determined by the longest relaxation time of a segment of wormlike micelle between two entanglement points which should roughly be equivalent to the mesh size in the entangled solution. In our experiments (Fig. 6) the bandwidth is not sufficient to go far beyond this crossover frequency into the asymptotic scaling regime, and the log-log slopes of G' and G'' are not constant for large enough intervals to make a precise statement about scaling exponents. Nevertheless, the superposition method we have presented above can still be used to infer the asymptotic scaling behavior, even if only the transition between regimes is captured in the data. This only works, however, if the transition takes place directly between two scaling regimes without other intervening complex dependencies. For entangled micelles one would expect the high-frequency single-filament behavior to be somewhere between that of flexible polymers and that of semiflexible polymers. For our system, the entanglement length was approximately 30 nm for $c_p=1\%$ while the persistence length was of order 10 nm. Semiflexible polymers show high-frequency scaling in the shear elastic modulus with an exponent of about 3/4 [5,6,43,44]. Our results point to a slightly lower exponent of about 0.67. There is no model to calculate the exact scaling behavior of a given polymer between the limits of semiflexible and flexible behavior, but an exponent of slightly less than 3/4 is reasonable. For Zimm dynamics, for a flexible chain including hydrodynamic effects, an exponent of about 5/9 is expected [36]. In the case of a chain with a persistence length somewhat larger than the monomer size assuming a more extended conformation, one might expect less of an effect from hydrodynamic interactions and therefore Rouse rather than Rouse-Zimm dynamics. For that case an exponent of 1/2 is expected. There may of course also be an influence of the particular dynamics of wormlike micelles that have so far not been considered. The breaking and reannealing dynamics might, for example, also influence the scaling exponent. The extraction of the scaling exponent from the transition regime data rests, as described, on the assumption that the transitions lead directly to the asymptotic high frequency scaling. A distinct possibility is that other dynamic regimes might follow the plateau regime before asymptotic scaling is reached [43]. Further experiments either with systems with intrinsically slower dynamics or of a similar system in a more viscous environment will be necessary to further explore high frequency rheology of wormlike micelle solutions.

[1] F. Ziemann, J. Radler, and E. Sackmann, Biophys. J. **66**, 2210 (1994).

[2] T. G. Mason and D. A. Weitz, Phys. Rev. Lett. **74**, 1250 (1995).

[3] F. Amblard, A. C. Maggs, B. Yurke, A. N. Pargellis, and S. Leibler, Phys. Rev. Lett. **77**, 4470 (1996).

[4] T. G. Mason, K. Ganesan, J. H. van Zanten, D. Wirtz, and S. C. Kuo, Phys. Rev. Lett. **79**, 3282 (1997).

[5] F. Gittes, B. Schnurr, P. D. Olmsted, F. C. MacKintosh, and C. F. Schmidt, Phys. Rev. Lett. **79**, 3286 (1997).

[6] B. Schnurr, F. Gittes, F. C. MacKintosh, and C. F. Schmidt, Macromolecules **30**, 7781 (1997).

[7] J. C. Crocker, M. T. Valentine, E. R. Weeks, T. Gisler, P. D. Kaplan, A. G. Yodh, and D. A. Weitz, Phys. Rev. Lett. **85**, 888 (2000).

[8] F. C. MacKintosh and C. F. Schmidt, Curr. Opin. Colloid Interface Sci. **4**, 300 (1999).

[9] L. D. Landau and E. M. Lifshitz, *Statistical Physics*, 3rd ed. (Butterworth and Heinemann, Oxford, 1980).

[10] A. Ashkin, Proc. Natl. Acad. Sci. U.S.A. **94**, 4853 (1997).

[11] T. M. Stokich, D. R. Radtke, C. C. White, and J. L. Schrag, J. Rheol. **38**, 1195 (1994).

[12] J. L. Schrag and R. M. Johnson, Rev. Sci. Instrum. **42**, 224 (1971).

[13] P. Hebraud, F. Lequeux, and J. F. Palierne, Langmuir **16**, 8296 (2000).

[14] A. J. Levine and T. C. Lubensky, Phys. Rev. E **63**, 041510 (2001).

[15] F. Brochard and P. G. Degennes, Macromolecules **10**, 1157 (1977).

[16] S. T. Milner, Phys. Rev. E **48**, 3674 (1993).

[17] L. D. Landau and E. M. Lifshitz, *Theory of Elasticity*, 3rd ed. (Butterworth and Heinemann, Oxford, 1986).

[18] D. T. Chen, E. R. Weeks, J. C. Crocker, M. F. Islam, R. Verma, J. Gruber, A. J. Levine, T. C. Lubensky, and A. G. Yodh, Phys. Rev. Lett. **90**, 108301 (2003).

[19] A. J. Levine and T. C. Lubensky, Phys. Rev. E **65**, 011501 (2002).

[20] L. M. Walker, Curr. Opin. Colloid Interface Sci. **6**, 451 (2001).

[21] R. Granek and M. E. Cates, J. Chem. Phys. **96**, 4758 (1992).

[22] J. F. Berret, J. Appell, and G. Porte, Langmuir **9**, 2851 (1993).

[23] M. E. Cates and S. J. Candau, J. Phys.: Condens. Matter **2**, 6869 (1990).

[24] H. Rehage and H. Hoffmann, J. Phys. Chem. **92**, 4712 (1988).

[25] D. Constantin, J. F. Palierne, E. Freyssingeas, and P. Oswald, Europhys. Lett. **58**, 236 (2002).

[26] F. Cardinaux, L. Cipelletti, F. Scheffold, and P. Schurtenberger, Europhys. Lett. **57**, 738 (2002).

[27] L. D. Landau and E. M. Lifshitz, *Fluid Mechanics*, 3rd ed. (Butterworth and Heinemann, Oxford, 1987).

[28] M. Cagnon and G. Durand, Phys. Rev. Lett. **45**, 1418 (1980).

[29] M. W. Allersma, F. Gittes, M. J. de Castro, R. J. Stewart, and C. F. Schmidt, Biophys. J. **74**, 1074 (1998).

[30] F. Gittes and C. F. Schmidt, Biophys. J. **74**, A183 (1998).

[31] E. J. G. Peterman, M. A. van Dijk, L. C. Kapitein, and C. F. Schmidt, Rev. Sci. Instrum. **74**, 3246 (2003).

[32] M. Atakhorrami, J. Kwiecinska, K. M. Addas, G. H. Koenderink, A. Levine, F. MacKintosh, and C. Schmidt (unpublished).

[33] E. J. G. Peterman, F. Gittes, and C. F. Schmidt, Biophys. J. **84**, 1308 (2003).

[34] F. Gittes and C. F. Schmidt, Methods Cell Biol. **55**, 129 (1998).

[35] M. S. Turner and M. E. Cates, Langmuir **7**, 1590 (1991).

[36] M. Doi and S. Edwards, *The Theory of Polymer Dynamics*, Vol. 73 of *International Series of Monographs on Physics* (Oxford Science Publications, Oxford, 1986).

[37] J. D. Ferry, *Viscoelastic Properties of Polymers* (Wiley, New York, 1980).

[38] V. Trappe and D. A. Weitz, Phys. Rev. Lett. **85**, 449 (2000).

[39] M. Gardel, J. Shin, F. MacKintosh, L. Mahadevan, P. Matsudaira, and D. Weitz, Phys. Rev. Lett. **93**, 188102 (2004).

[40] L. Starrs and P. Bartlett, J. Phys.: Condens. Matter **15**, S251 (2003), sp. Iss. SI.

[41] K. M. Addas, M. Atakhorrami, J. X Tang, A. Levine, F. C. MacKintosh, and C. F. Schmidt (unpublished).

[42] M. Atakhorrami, G. H. Koenderink, F. MacKintosh, and C. Schmidt (unpublished).

[43] D. C. Morse, Phys. Rev. E **58**, R1237 (1998), part A.

[44] F. Gittes and F. C. MacKintosh, Phys. Rev. E **58**, R1241 (1998).